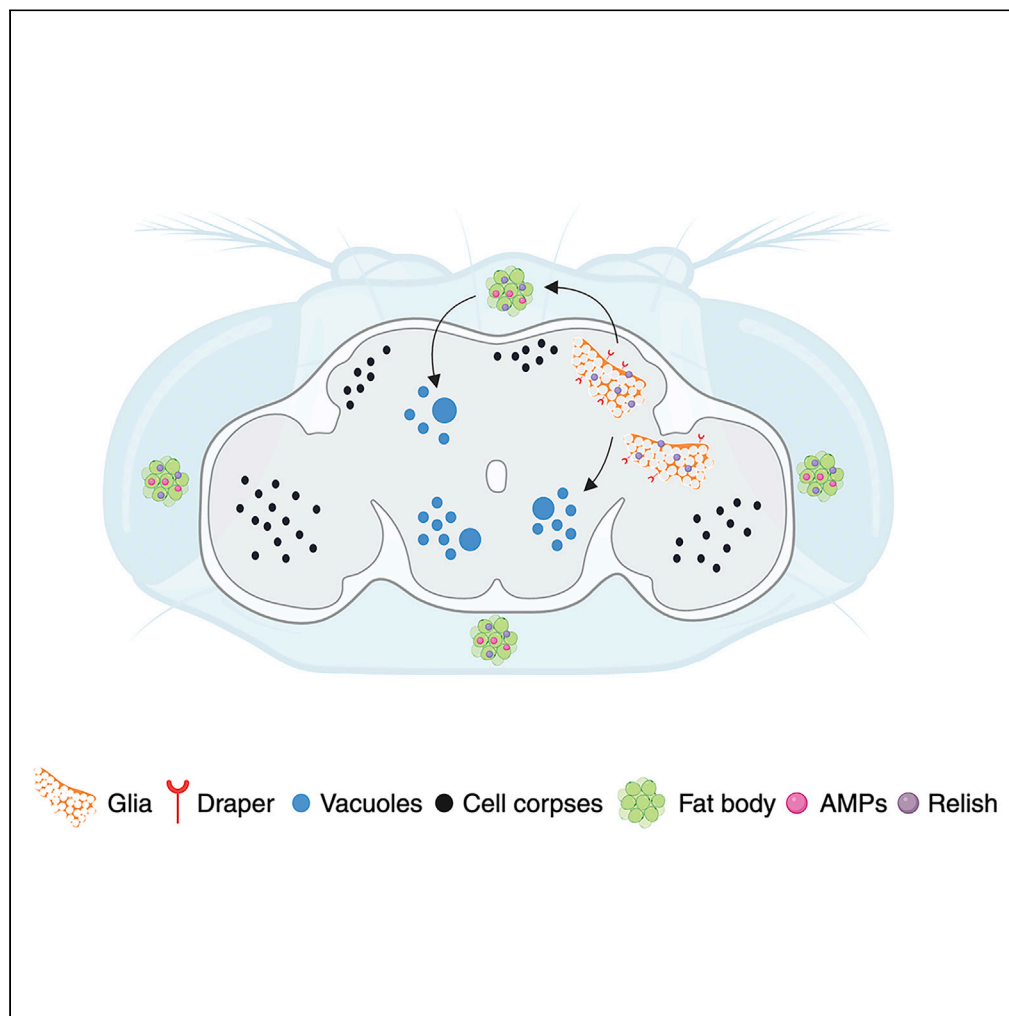


Article

Defective phagocytosis leads to neurodegeneration through systemic increased innate immune signaling



Johnny E. Elguero,
Guangmei Liu,
Katherine
Tiemeyer, ...,
Lauren Duro,
Zhenhao Yan,
Kimberly McCall

kmccall@bu.edu

Highlights

Loss of Draper phagocytic receptor leads to dysregulation of immune signaling

Draper mutants show the upregulation of *AttacinA* in the pericerebral fat body

Inhibition of the Imd pathway leads to reduced neurodegeneration in *draper* mutants

The Imd pathway acts locally in glia and systemically to promote neurodegeneration

Elguero et al., iScience 26,
108052
October 20, 2023 © 2023 The
Authors.
[https://doi.org/10.1016/
j.isci.2023.108052](https://doi.org/10.1016/j.isci.2023.108052)

Article

Defective phagocytosis leads to neurodegeneration through systemic increased innate immune signaling

Johnny E. Elguero,^{1,2} Guangmei Liu,^{1,2} Katherine Tiemeyer,¹ Shruthi Bandyadka,¹ Heena Gandevia,¹ Lauren Duro,¹ Zhenhao Yan,¹ and Kimberly McCall^{1,3,*}

SUMMARY

In nervous system development, disease, and injury, neurons undergo programmed cell death, leaving behind cell corpses that are removed by phagocytic glia. Altered glial phagocytosis has been implicated in several neurological diseases including Alzheimer's disease. To untangle the links between glial phagocytosis and neurodegeneration, we investigated *Drosophila* mutants lacking the phagocytic receptor Draper. Loss of Draper leads to persistent neuronal cell corpses and age-dependent neurodegeneration. Here we investigate whether the phagocytic defects observed in *draper* mutants lead to chronic increased immune activation that promotes neurodegeneration. We found that the antimicrobial peptide Attacin-A is highly upregulated in the fat body of aged *draper* mutants and that the inhibition of the Immune deficiency (Imd) pathway in the glia and fat body of *draper* mutants led to reduced neurodegeneration. Taken together, these findings indicate that phagocytic defects lead to neurodegeneration via increased immune signaling, both systemically and locally in the brain.

INTRODUCTION

The link between neurodegeneration and innate immunity has been the subject of much research in recent years.^{1–4} Innate immunity consists of two main branches: the cellular branch, or phagocytosis, and the humoral branch, which is comprised of signaling pathways culminating in the release of cytokines, antimicrobial peptides (AMPs), and other immune molecules.^{5,6} One aspect of innate immunity, inflammation, can be defined as the activation of immune cells coupled with the release of inflammatory cytokines. This response is important for the protection of the organism from pathogens as well as for tissue repair after injury. Although inflammation is protective in the context of infection and injury, chronic inflammation is known to be detrimental.^{7,8} The presence of inflammation in the central nervous system has been termed “neuroinflammation,” and typically refers to the presence of activated, pro-inflammatory microglia and astrocytes as well as infiltrating peripheral immune cells.^{9,10}

In humans, the presence of inflammatory microglia is associated with both aging and neurodegenerative conditions^{11,12} and in mammals and *Drosophila*, increased innate immune signaling has been shown to induce or worsen neurodegeneration.^{1,7,8,13} *Drosophila* do not have microglia, but phagocytosis of neuronal processes and dead cells is carried out by other types of glia. The presence of uncleared cell corpses and debris is thought to lead to increased immune signaling¹⁴ and glial phagocytic ability is known to decrease with age in both mammals and *Drosophila*.^{15,16} Thus, in aging, a lack of phagocytosis may contribute to increased neuroinflammation through the persistence of uncleared material that may in turn worsen neurodegeneration.

The humoral immune response in *Drosophila* is mediated primarily by two NF- κ B signaling pathways, Toll and Immune deficiency (Imd).^{5,6,17} These pathways activate the transcription of antimicrobial peptides (AMPs) primarily in the fat body, a tissue with similarities to the vertebrate liver. However, there are additional complexities to these immune pathways. While AMPs are known to target bacteria and fungi, they have also been shown to contribute to neurodegeneration and other processes.^{5,7} Moreover, the Toll and Imd pathways activate the transcription of other genes, are expressed in multiple tissues and act in concert with other pathways and phagocytic cells to remove invading pathogens.^{5,17}

The basic steps of phagocytosis are conserved across species.^{18–20} In *Drosophila*, Draper is a major phagocytic receptor with roles in phagocytosis of bacteria, debris, and apoptotic cells throughout the body. In the brain, Draper has been shown to function in glia during the pruning of axons, clearance after axotomy, and in the removal of apoptotic cells.²¹ The absence of Draper in the brain leads to the

¹Department of Biology, Boston University, 5 Cummington Mall, Boston, MA 02115, USA

²These authors contributed equally

³Lead contact

*Correspondence: kmccall@bu.edu

<https://doi.org/10.1016/j.isci.2023.108052>



persistence of neuronal corpses^{22–24} and age-dependent neurodegeneration.^{23,25} However, the mechanisms by which the loss of Draper leads to neurodegeneration have yet to be determined.

Here we address whether the inhibition of the cellular innate immune response, via mutants lacking the phagocytic receptor Draper, results in an overactivation of the humoral response. Specifically, we hypothesized that the absence of phagocytosis and the presence of uncleared corpses would lead to increased innate immune signaling which would promote neurodegeneration. Indeed, we found elevated expression of anti-microbial peptides in the *draper* mutant, and found that suppression of the Imd pathway in either glia or fat body could reduce neurodegeneration in *draper* mutants. Taken together, these findings indicate that phagocytic defects lead to neurodegeneration through increased immune signaling, both systemically and locally in the brain.

RESULTS

Aged *draper* mutants display the dysregulation of anti-microbial peptide expression

To determine if innate immune signaling was affected in mutants lacking the phagocytic receptor Draper (*drpr*^{Δ5}), we extracted RNA from whole heads and performed RT-qPCR for three representative anti-microbial peptides: Attacin-A (*AttA*), Attacin-D (*AttD*), and Diptericin (*Dipt*). We found that at an early age (5 days post-eclosion), *AttA* mRNA expression trended toward elevation in *drpr*^{Δ5} heads, as compared to control heads (Figure 1A). At 14 days post-eclosion, this increase was more pronounced, with an average increase of around 700-fold as compared to 5-day old control flies. At 40 days post-eclosion, *AttA* expression in *drpr*^{Δ5} mutants showed an increase of over 1500-fold as compared to 5-day old control flies. In contrast, 40-day old control flies showed an increase of about 14-fold compared to 5-day old flies. While *AttD* expression showed an increasing trend as *drpr*^{Δ5} flies aged, this change was not significant (Figure 1B). *Dipt* expression similarly showed an increasing trend, but no significant change with age, and the increase appeared to be similar in control flies (Figure 1C). Similarly, we found the dysregulation of AMPs when *draper* was knocked down specifically in glia (Figure S1). Taken together, these experiments suggest that innate immune signaling, particularly *AttA* expression, is drastically altered in *drpr*^{Δ5} mutant heads. However, as RT-qPCR involved extracting RNA from whole heads and not a specific tissue, we were not able to ascertain whether the observed dysregulated AMP expression could be attributed to the brain or another tissue in the head.

Attacin-GFP is expressed in neurons in young and aged, control and *draper* mutant brains at similar levels

To determine whether the dysregulation of AMP expression we observed in fly heads resulted specifically from brain expression, we used flies carrying the genetic reporter *AttGFP*, which contains the 2.4 kb regulatory region of *AttA* upstream of GFP and has been shown to report *AttA* expression.²⁶ We first dissected brains of *AttGFP* flies and identified several cells in the brain that expressed *AttA* (Figures S2A'–S2B', arrowheads). Co-labeling with anti-Repo antibody to mark glia (Figures S2A''–S2B''') revealed that these cells were not glia. However, co-labeling with anti-Elav antibody to mark neurons (Figures S2C–S2D''') confirmed that most *AttGFP*-expressing cells were neurons. We then dissected young and aged *AttGFP* and *AttGFP drpr*^{Δ5} flies to determine whether the upregulation of *AttA* observed in *drpr*^{Δ5} mutants through RT-qPCR resulted from brain expression. In young flies, *AttGFP drpr*^{Δ5} brains did not show a noticeable upregulation in *AttA* expression as compared to *AttGFP* brains (Figures 2A and 2B'). We then dissected the brains of flies aged to 40 days, and found once again that *AttA* expression was not noticeably different between *AttGFP* brains and *AttGFP drpr*^{Δ5} brains (Figures 2C–2D'). Thus, we concluded that the increase in *AttA* expression in aged *drpr*^{Δ5} mutants observed through RT-qPCR did not result from expression in the brain.

Attacin-GFP expression is increased in the aged *drpr* mutant fat body

To visualize *AttA* expression in tissues other than the brain, we cryosectioned whole heads of *AttGFP* and *AttGFP drpr*^{Δ5} flies. We used tissue morphology, nuclear labeling by DAPI, and anatomical location to identify fat body tissue, brain tissue, and eyes in head sections (Figures 3B and 3B'). The fat body was a tissue of particular interest, as it is associated with immune signaling. We used BODIPY, which labels lipids (Figure 3A), to distinguish the pericerebral fat body from other tissues surrounding the brain. As observed in the dissection of whole brains (Figure 2), there was no difference in *AttGFP* expression in the brain between any groups observed in cryosections (Figures 3C–3F). We thus turned our attention to the pericerebral fat body. We found that in young flies (1–2 days post-eclosion), there was no difference in *AttA* expression between *AttGFP* (control) flies (Figure 3C) and *AttGFP drpr*^{Δ5} flies (Figure 3D). However, in aged flies, both *AttGFP* (Figure 3E) and *AttGFP drpr*^{Δ5} (Figure 3F) showed an increase in *AttGFP* expression in the pericerebral fat body. While this increase was present in some of the sections from *AttGFP* flies, it was present in all sections from *AttGFP drpr*^{Δ5} (*n* = 7 flies). The percentage of GFP-positive pericerebral fat body was quantified in several sections per head, and we found a highly significant increase in *AttA* expression in aged, but not young, *drpr* mutants, compared to age-matched controls (Figure 3G).

We next determined whether the increase in *AttA* expression was specific to the pericerebral fat body or if it was a systemic effect. We cryosectioned whole bodies of *AttGFP* and *AttGFP drpr*^{Δ5} flies and stained with anti-GFP antibody to visualize *AttA* expression. We used cell morphology and anatomical location to identify fat body cells in the abdomen. As with the pericerebral fat body, expression of *AttA* in the abdominal fat body was unchanged between the young *AttGFP* control flies (Figures S3A–S3A'') and *AttGFP drpr*^{Δ5} flies (Figures S3B–S3B''). In 40-day old flies, there was an increase in *AttA* expression between *AttGFP* control flies (Figures S3C–S3C'') and *AttGFP drpr*^{Δ5} flies (Figures S3D–S3D''). However, this increase was not consistent across all samples where some abdomens did not show an increase in *AttA* expression (Figures S3E–S3E''). This suggests that the upregulation of immune signaling was more pronounced in the head of *drpr* mutants.

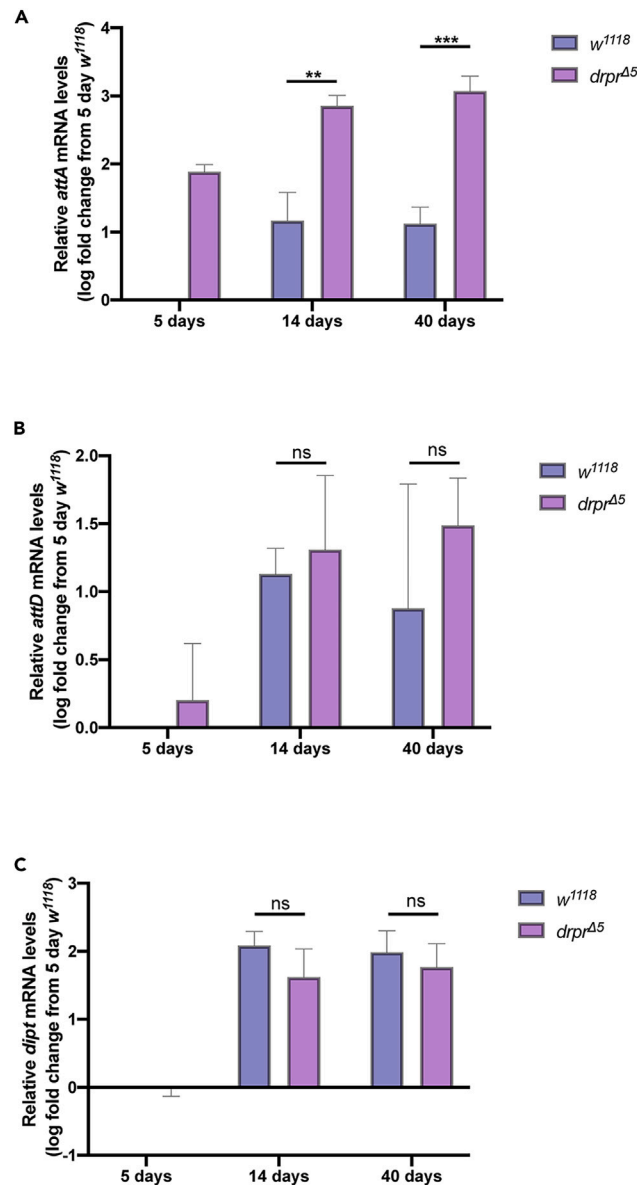


Figure 1. RT-qPCR shows the dysregulation of innate immunity in *drpr⁴⁵* mutants

(A–C) Log fold change in expression of *AttA* (A), *AttD* (B), and *dpt* (*DptA*) (C) in whole heads of *drpr⁴⁵* or *w¹¹¹⁸* flies, as compared to 5-day old *w¹¹¹⁸*, is shown. $n = 30$ flies per sample. Values shown are mean \pm S.D. Unpaired t-tests with Welch correction were performed using Prism software. * $p < 0.05$, ** $p < 0.01$, *** $p < 0.001$. See also [Figure S1](#).

Glial and fat-body, but not neuronal, knockdown of *Relish* in *draper* mutants attenuates neurodegeneration

To determine whether the neurodegeneration observed in *drpr⁴⁵* mutants is mediated by an overactive immune response, we genetically inhibited the Imd pathway in neurons, glia, or fat body cells in a *drpr⁴⁵* mutant background by expressing dsRNA targeting the NF- κ B transcription factor *Relish* using Gal4 drivers specific to these cell types. We then aged the flies and performed cryosectioning to measure levels of vacuolization, a hallmark of neurodegeneration in *Drosophila*.^{27–30} We found, as expected, that *drpr⁴⁵* mutants carrying only the GAL4 drivers showed high levels of neurodegeneration compared to controls ([Figures 4A–4F](#) and [4J](#)). *drpr⁴⁵* mutants expressing *Relish* RNAi in neurons with *elav-Gal4* did not show decreased levels of neurodegeneration ([Figures 4I](#) and [4J](#)). *drpr⁴⁵* mutants carrying only the fat body driver *ppl-GAL4* showed high levels of neurodegeneration but *drpr⁴⁵* mutants expressing *Relish* RNAi in the fat body showed significantly less vacuolization ([Figures 4E](#), [4H](#) and [4J](#)). Similarly, inhibiting *Relish* in glia with *repo-GAL4* in a *drpr⁴⁵* mutant background significantly reduced the level of vacuolization, as compared to *drpr⁴⁵* mutants carrying only the glial driver ([Figures 4D](#), [4G](#) and [4J](#)). Simultaneous knockdown of *drpr* and *Relish* in glia also led to reduced vacuolization compared to *drpr* knockdown alone, although the effect did not reach statistical significance with a small sample size

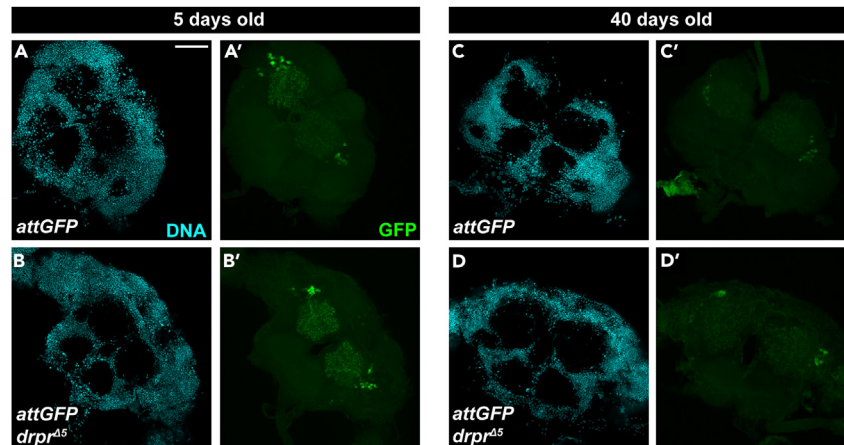


Figure 2. Brain expression of AttA is unchanged in aged *drpr*⁴⁵ mutants

(A–A') Representative images of 5-day old AttGFP brain stained with DAPI (A) and anti-GFP (A').

(B–B') Representative images of 5-day old AttGFP, *drpr*⁴⁵ brain stained with DAPI (B) and anti-GFP (B').

(C–D') Representative images of 40-day old AttGFP (C–C') or AttGFP, *drpr*⁴⁵ (D–D') brain stained with DAPI (C, D) and anti-GFP (C', D'). Scale bar = 50 μ m. See also Figure S2.

(Figure S4). Moreover, dopaminergic neuron loss in *drpr*⁴⁵ mutants was suppressed by inhibiting *Relish* in glia or fat body but not neurons (Figure 5). Taken together, these findings indicate that the activation of the Imd pathway in glia and fat body, but not neurons, contributes to neurodegeneration seen in the *drpr*⁴⁵ mutant. As AttA upregulation was not observed in glia (Figures S2A–S2B'') and knockdown of its transcription factor, *Relish*, in glia attenuates neurodegeneration in the *drpr* mutants (Figure 4), it is likely that *Relish* has different targets other than AttA in glia that promote neurodegeneration. Alternatively, there may be common targets or downstream effectors of *Relish* which are released from both fat body and glia and can also cross the blood–brain barrier from the peripheral fat body to the brain. It is also possible that there may be crosstalk between the fat body and glia, and/or the pathways promoting neurodegeneration may be different in the fat body and glia.

We previously found that the inhibition of the TORC1 or autophagy pathway also suppressed neurodegeneration in *draper* mutants, and this was accompanied by a pronounced reduction in the persistence of neuronal corpses.²³ To determine if *Relish* also suppressed corpse persistence, we performed TUNEL labeling to detect apoptotic cells in the brain. We detected a modest reduction in the number of TUNEL-positive cells in all of the genotypes expressing *Relish* (Figure 6), but the number of corpses remained very high (600+ per central brain) compared to less than 100 in the TORC1-inhibited flies.²³ Thus, we conclude that the mechanism of suppression of neurodegeneration in *draper* mutants is distinct in TORC1 vs. *Relish* inhibited flies. We propose that *Relish* primarily affects neurodegeneration downstream of corpse persistence and the major effect of *Relish* knockdown is not to affect phagocytosis or phagosome maturation in the *draper* mutant.

DISCUSSION

Chronic activation of innate immunity in the brain is known to play a role in neurodegenerative disease progression, although the mechanisms underlying this role remain unclear. Microglia, the resident macrophages of the mammalian brain, can become “activated,” releasing pro-inflammatory cytokines and reactive oxygen species, damaging nearby neurons.³¹ However, “activated” microglia are also thought to be protective at times, clearing dead cells, cellular debris, and disease-associated protein aggregates.^{32,33} Interestingly, in aging, the phagocytic abilities of microglia decrease, while their pro-inflammatory reactivity increases.¹⁶ This interplay between phagocytosis and innate immunity in the brain remains poorly understood. In *Drosophila*, recent findings have suggested that increased innate immune signaling in the brain is similarly detrimental.^{7,8,13} As we and others have shown, phagocytic defects in *Drosophila* glia lead to age-dependent neurodegeneration.^{23,25} Thus, *Drosophila* provide a useful model in which to untangle the links between glial phagocytosis, innate immune signaling, and neurodegeneration.

As increased innate immune signaling is thought to cause or worsen neurodegeneration, and the presence of uncleared cell corpses and debris is thought to lead to the activation of innate immunity, we hypothesized that the neurodegeneration observed in *drpr*⁴⁵ flies could be caused by overactive innate immune signaling. Thus, we first measured AMP expression as a readout for the Imd pathway and found that AttA was upregulated in the aged *drpr*⁴⁵ mutant head. We then used cryosectioning to identify which tissue was responsible for the elevated AttA expression and found that this upregulation was primarily the result of expression in the fat body. Interestingly, glial-specific knockdowns of *drpr* did not show the same effect on AttA, although other AMPs were increased. This suggests that loss of *drpr* from other tissues in the fly also contributes to immune dysregulation.

To determine whether this overactive immune signaling was contributing to neurodegeneration, we knocked down *Relish* in the fat body, glia, and neurons in the *drpr*⁴⁵ mutant and measured neurodegeneration. We found that inhibiting the Imd pathway in the glia and fat body, but not neurons, partially suppressed neurodegeneration in the *drpr*⁴⁵ mutant. These findings suggest that increased innate immune activity, both systemically and in glia, drive neurodegeneration in the *drpr*⁴⁵ mutant. Interestingly, the effect on neurodegeneration was more modest

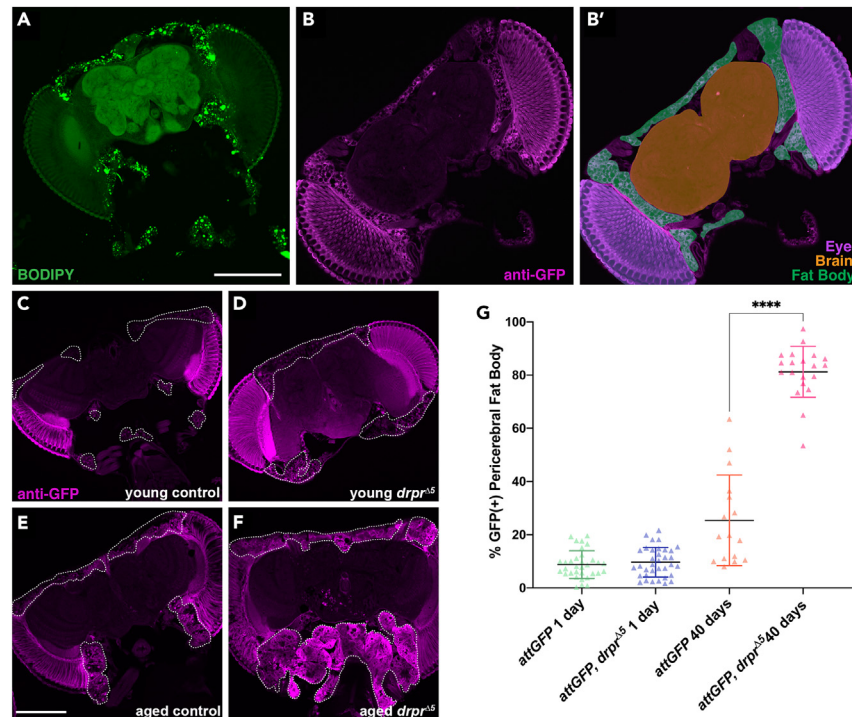


Figure 3. Pericerebral fat body expression of AttA is increased in aged *drpr* mutants

(A) BODIPY staining (lipids) was used for the positive identification of fat body cells in cryosectioned *Drosophila* heads. (B–B') Cryosection of *AttGFP* fly head stained with anti-GFP (magenta, B), with brain, eyes, and fat body highlighted in orange, purple, and green, respectively (B'). (C and D) Representative sections of young *AttGFP* (C) and *AttGFP drpr^{Δ5}* (D) heads, stained with anti-GFP (magenta), showing no difference in *AttA* expression. Dotted white line surrounds regions of fat body. (E and F) Representative sections of aged *AttGFP* (E) and *AttGFP drpr^{Δ5}* (F), stained with anti-GFP (magenta), showing increased *AttA* expression in *drpr^{Δ5}* pericerebral fat body. Scale bars = 100 μ m. (G) Quantification of GFP-positive pericerebral fat body in young and aged *AttGFP* and *AttGFP drpr^{Δ5}* flies. Sections were quantified from 3 replicate experiments (*AttGFP* young n = 8 flies, *AttGFP drpr^{Δ5}* young n = 9, *AttGFP* aged n = 10, *AttGFP drpr^{Δ5}* n = 7). Values shown are mean \pm S.D. Unpaired t-tests were performed using Prism software. ****p < 0.0001. See also Figure S3.

with *drpr* RNAi knockdown in glia, suggesting that loss of *drpr* throughout the body could contribute to neurodegeneration, although we cannot rule out the more modest effect being due to a partial knockdown with RNAi.

A previous study found that increased activation of the Imd pathway can induce age-dependent neurodegeneration.⁷ Mutations in the *dnr1* (*defense repressor 1*) gene, a negative regulator of the Imd pathway, result in increased immune signaling and neurodegeneration. The authors also induced AMP expression in the brain, both genetically and by bacterial injection, and found this sufficient to cause neurodegeneration.⁷ Interestingly, when the authors activated systemic innate immunity by injecting bacteria into the thorax, they did not see neurodegeneration. The authors state that this is because AMPs are not expected to cross the blood-brain barrier. Our finding that suppressing systemic immunity is sufficient to attenuate neurodegeneration suggests the possibility that some AMPs do cross the blood-brain barrier, or that systemic innate immunity can be neurotoxic in other ways. It is possible that the *drpr^{Δ5}* mutant has increased blood-brain barrier permeability, although to our knowledge this has not been investigated. Due to the nature of the *AttGFP* reporter, we were only able to visualize the transcriptional regulation of *AttA*, rather than the localization of the peptide.

In humans, systemic inflammation can occur chronically or acutely, driven by underlying causes such as infection, chronic illness, and aging. Cytokines and other pro-inflammatory mediators can affect the brain by crossing the blood-brain barrier or entering the circumventricular organs.^{34,35} Systemic inflammation is thought to induce the activation of glia, leading to inflammation in the CNS.³⁶ In aged or diseased brains, glia are thought to be primed in a way that makes them more reactive to stimuli capable of inducing a pro-inflammatory state.³⁷ Chronic, low-level systemic inflammation is also thought to play an important role in neurodegenerative disease. Evidence for this comes from long-term studies showing that factors known to increase levels of inflammation, such as smoking, obesity, vascular disease, and periodontal disease increase the risk of neurodegenerative disease.^{38,39} Additionally, long-term use of NSAIDs reduces the risk of AD, suggesting that maintaining low levels of systemic inflammation earlier in life can be protective.⁴⁰

Our study identifies a source of systemic inflammation in *Drosophila*: defective phagocytosis. Whether this results from the persistence of apoptotic corpses, debris, pathogens, or another mechanism remains unclear. Our finding that the inhibition of immune signaling in glia attenuated neurodegeneration suggests that elevated systemic immune signaling may drive neurodegeneration through the activation of glia, as is

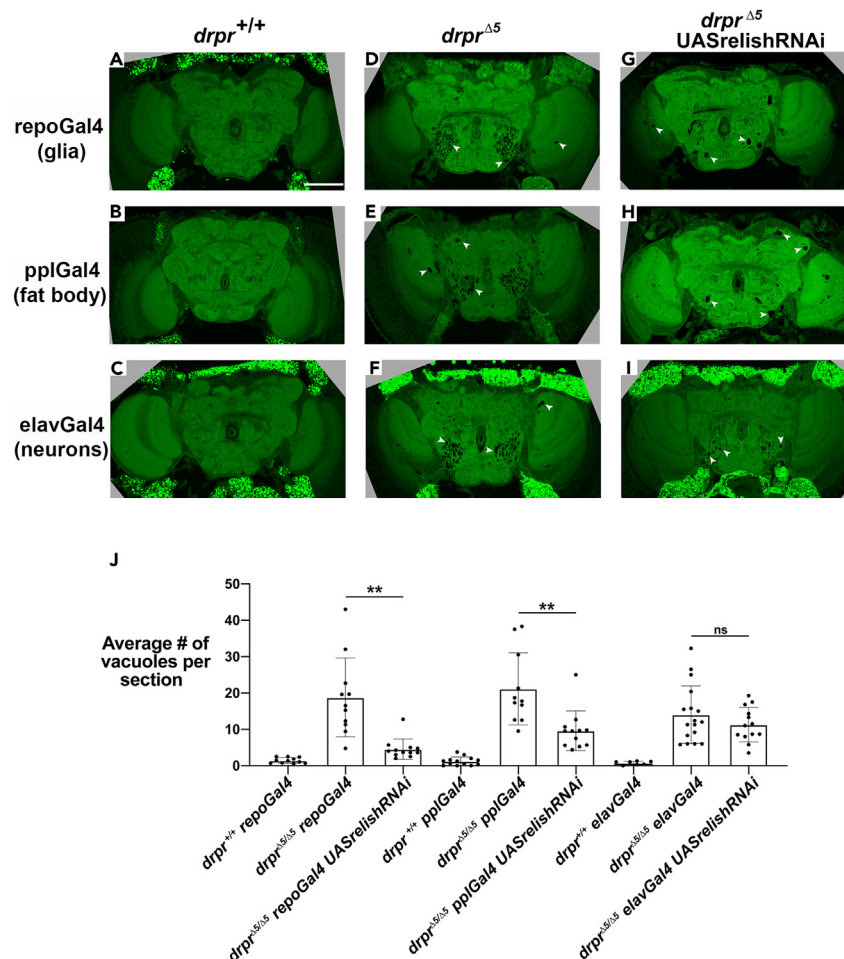


Figure 4. Knockdown of *Relish* in glia and fat body, but not neurons, attenuates neurodegeneration in *drpr* mutant flies

(A–C) Representative sections of 40-day old *drpr^{+/+}* flies carrying the glial driver *repo-Gal4* (A), the fat body driver *ppl-Gal4* (B), or the neuronal driver *elav-Gal4*, stained with BODIPY.

(D–F) Representative sections of 40-day old *drpr^{Δ5}* flies carrying *repo-Gal4* (D), *ppl-Gal4* (E), or *elav-Gal4* (F) stained with BODIPY. White arrowheads point to vacuolar lesions.

(G–I) Representative sections of 40-day old *drpr^{Δ5}* flies with *Relish-RNAi* expressed in glia (G), fat body (H), or neurons (I). White arrowheads point to vacuolar lesions. Scale bar = 100 μ m.

(J) Average number of vacuolar lesions per section for each genotype. Each dot represents one head, with at least two sections analyzed per head. Brown-Forsythe and Welch ANOVA and unpaired t tests with Welch correction were performed using Prism software. p-values shown for unpaired t tests with Welch correction. **p < 0.01. See also Figure S4.

thought to be the case in mammals. In *Drosophila*, the activation of glia has primarily been described in the context of phagocytic clearance of injured axons.⁴¹ Whether glia engage in other pro-inflammatory signaling remains unclear, although Imd signaling has been reported in glia.^{7,42} While we did not see elevated expression of *AttA* in glia in the *drpr^{Δ5}* mutant, *Relish* regulates the expression of many genes including other AMPs.¹⁷ It is also possible that *Relish* may activate target genes that can directly affect phagocytosis, since we found a modest reduction in the number of persisting corpses in *drpr* mutants when *Relish* was knocked down (Figure 6). Future identification of these key transcriptional targets of *Relish* will provide insight into how local and systemic immune signaling drives neuroinflammation and neurodegeneration in *Drosophila*.

Limitations of the study

Our study reports the role of immune signaling in the fat body and glia in promoting neurodegeneration in *draper* phagocytosis-defective mutants. While we found an upregulation of *AttA* in the fat body, we did not determine a requirement for *AttA* or other targets of *Relish* in neurodegeneration in this context, and further study will be needed to identify the relevant targets of *Relish*. Additionally, we found that knockdown of *drpr* in glia led to more modest effects than the null mutant on immune signaling and neurodegeneration, but we did not determine if this is due to an incomplete knockdown or if loss of *drpr* in the periphery promotes neurodegeneration. Further studies are needed to decipher the interactions between peripheral tissues and the brain in promoting neurodegeneration.

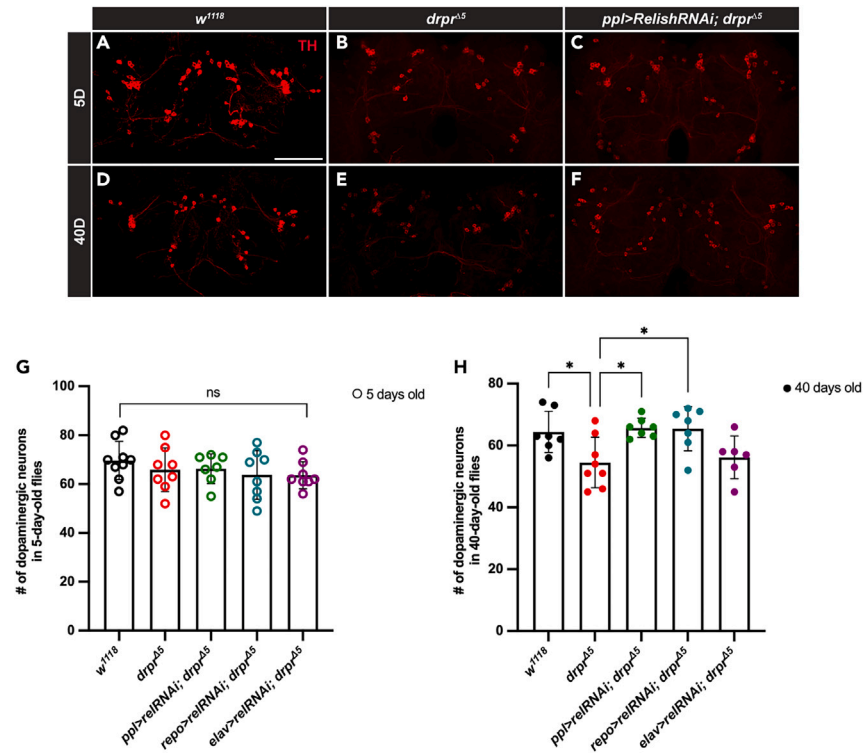


Figure 5. Knockdown of *Relish* in glia and fat body, but not neurons, attenuates dopaminergic neuron loss in *drpr* mutant flies

(A–C) Representative projection images of brains with dopaminergic neurons labeled with anti-tyrosine hydroxylase from the posterior region (~31 μm thick) of whole-mount 5-day old *w¹¹¹⁸* flies (A), *drpr^{d5}* flies (B) and *drpr^{d5}* flies expressing *Relish RNAi* in fat body (C).

(D–F) Representative images of brains from 40-day old *w¹¹¹⁸* flies (D), *drpr^{d5}* flies (E) and *drpr^{d5}* flies expressing *Relish RNAi* in fat body (F). Scale bar = 50 μm.

(G) The total number of dopaminergic neurons within confocal stacks (30 μm) of 5-day old *w¹¹¹⁸* flies, *drpr^{d5}* flies and *drpr^{d5}* flies with *Relish RNAi* expressed in fat body (*pp1*), glia (*repo*) or neurons (*elav*). Values shown are mean ± S.D. n ≥ 6.

(H) The total number of dopaminergic neurons within confocal stacks (30 μm) of 40-day old flies. Each dot represents one brain. Values shown are mean ± S.D. n ≥ 6. One-way ANOVA with Dunnett's posttest was performed using Prism software. n.s., not significant, *p < 0.05.

STAR★METHODS

Detailed methods are provided in the online version of this paper and include the following:

- KEY RESOURCES TABLE
- RESOURCE AVAILABILITY
 - Lead contact
 - Materials availability
 - Data and code availability
- EXPERIMENTAL MODEL AND SUBJECT DETAILS
 - Fly stocks and husbandry
- METHOD DETAILS
 - Dissection and histology
 - Staining procedures
 - TUNEL staining
 - Microscopy
 - RT-PCR
- QUANTIFICATION AND STATISTICAL ANALYSIS

SUPPLEMENTAL INFORMATION

Supplemental information can be found online at <https://doi.org/10.1016/j.isci.2023.108052>.

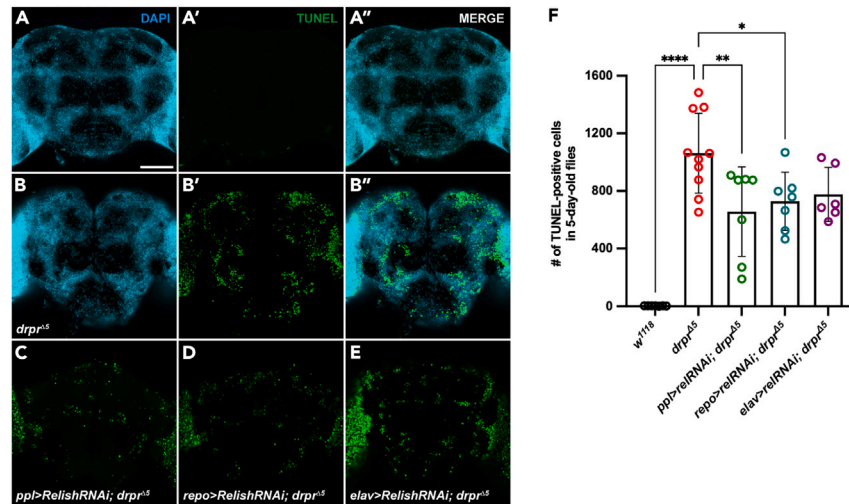


Figure 6. Knockdown of *Relish* leads to a reduction of cell corpses in *drpr* mutant flies

(A–A'') Representative projection images of brains with cell corpses labeled with DAPI (A), TUNEL (A') and merged channels (A'') from the anterior region (30 μ m thick) of whole-mount 5-day old *w¹¹¹⁸* flies. Scale bar = 50 μ m.

(B–B'') Representative brain images labeled with DAPI (B), TUNEL (B') and merged channels (B'') from 5-day old *drpr^{Δ5}* flies.

(C–E) Representative brain images of 5-day old *drpr^{Δ5}* flies with *Relish* RNAi expressed in fat body (C), glia (D) or neurons (E).

(F) The total number of TUNEL-positive cell corpses within confocal stacks (30 μ m) of 5-day old flies. Each dot represents one brain. Values shown are mean \pm S.D. $n \geq 6$. One-way ANOVA with Dunnett's posttest was performed using Prism software. * $p < 0.05$, ** $p < 0.01$, **** $p < 0.0001$.

ACKNOWLEDGMENTS

We thank Mel Feany, Susan Holmes, Angela Ho, Tuan Leng Tay, and members of our laboratory for helpful discussions and comments on the article. We thank JiSoo Park and Cheng Yang Shi for technical assistance. We thank Ian Davison for assistance with 2-photon microscopy. We thank the Vienna and Bloomington *Drosophila* Stock Centers, Mitch Dushay, Mary Logan, Marc Freeman, and Michael O'Connor for generously providing fly strains, and the Developmental Studies Hybridoma Bank for antibodies. Stocks obtained from the Bloomington *Drosophila* Stock Center (NIH P40OD018537) were used in this study. We thank our funding sources: NIH Grants R21 AG056158 and R35 GM127338 to KM, the Beckman Foundation to KT and UROP at Boston University to LD and ZY.

AUTHOR CONTRIBUTIONS

Conceptualization: JEE, KM, and GL; methodology: JEE, GL, and SB; investigation: JEE, GL, HG, KT, SB, ZY, LD, and KM; writing: JEE, GL, SB, and KM; funding acquisition: KM, supervision: KM.

DECLARATION OF INTERESTS

The authors declare no conflicts of interest.

INCLUSION AND DIVERSITY

We support inclusive, diverse, and equitable conduct of research.

Received: November 28, 2022

Revised: August 1, 2023

Accepted: September 22, 2023

Published: September 26, 2023

REFERENCES

- Pluvinage, J.v., and Wyss-Coray, T. (2020). Systemic factors as mediators of brain homeostasis, ageing and neurodegeneration. *Nat. Rev. Neurosci.* 21, 93–102. <https://doi.org/10.1038/s41583-019-0255-9>.
- Nainu, F., Salim, E., Asri, R.M., Hori, A., and Kuraishi, T. (2019). Neurodegenerative disorders and sterile inflammation: Lessons from a *Drosophila* model. *J. Biochem.* 166, 213–221. <https://doi.org/10.1093/jb/mvz053>.
- Dhankhar, J., Agrawal, N., and Shrivastava, A. (2020). An interplay between immune response and neurodegenerative disease progression: An assessment using *Drosophila* as a model. *J. Neuroimmunol.* 346, 577302.

- <https://doi.org/10.1016/j.jneuroim.2020.577302>.
- Mason, H.D., and McGavern, D.B. (2022). How the immune system shapes neurodegenerative diseases. *Trends Neurosci.* 45, 733–748. <https://doi.org/10.1016/j.tins.2022.08.001>.
 - Yu, S., Luo, F., Xu, Y., Zhang, Y., and Jin, L.H. (2022). *Drosophila* Innate Immunity Involves Multiple Signaling Pathways and Coordinated Communication Between Different Tissues. *Front. Immunol.* 13, 905370. <https://doi.org/10.3389/fimmu.2022.905370>.
 - Buchon, N., Silverman, N., and Cherry, S. (2014). Immunity in *Drosophila melanogaster* from microbial recognition to whole-organism physiology. *Nat. Rev. Immunol.* 14, 796–810. <https://doi.org/10.1038/nri3763>.
 - Cao, Y., Chtarbanova, S., Petersen, A.J., and Ganetzky, B. (2013). *Dnr1* mutations cause neurodegeneration in *Drosophila* by activating the innate immune response in the brain. *Proc. Natl. Acad. Sci. USA* 110, E1752–E1760. <https://doi.org/10.1073/pnas.1306220110>.
 - Kounatidis, I., Chtarbanova, S., Cao, Y., Hayne, M., Jayanth, D., Ganetzky, B., and Ligoxygakis, P. (2017). NF- κ B Immunity in the Brain Determines Fly Lifespan in Healthy Aging and Age-Related Neurodegeneration. *Cell Rep.* 19, 836–848. <https://doi.org/10.1016/j.celrep.2017.04.007>.
 - Kölliker-Frers, R., Udovin, L., Otero-Losada, M., Kobic, T., Herrera, M.I., Palacios, J., Razzitte, G., and Capani, F. (2021). Neuroinflammation: An Integrating Overview of Reactive-Neuroimmune Cell Interactions in Health and Disease. *Mediat. Inflamm.* 2021. <https://doi.org/10.1155/2021/9999146>.
 - Paolicelli, R.C., Sierra, A., Stevens, B., Tremblay, M.E., Aguzzi, A., Ajami, B., Amit, I., Audinat, E., Bechmann, I., Bennett, M., et al. (2022). Microglia states and nomenclature: A field at its crossroads. *Neuron* 110, 3458–3483. <https://doi.org/10.1016/j.neuron.2022.10.020>.
 - Manjally, A.V., and Tay, T.L. (2022). Attack of the Clones: Microglia in Health and Disease. *Front. Cell. Neurosci.* 16, 831747. <https://doi.org/10.3389/fncel.2022.831747>.
 - Cornejo, F., and von Bernhard, R. (2016). Age-dependent changes in the activation and regulation of microglia. *Adv. Exp. Med. Biol.* 949, 205–226. https://doi.org/10.1007/978-3-319-40764-7_10.
 - Petersen, A.J., Katzenberger, R.J., and Wassarman, D.A. (2013). The innate immune response transcription factor relish is necessary for neurodegeneration in a *Drosophila* model of ataxia-telangiectasia. *Genetics* 194, 133–142. <https://doi.org/10.1534/genetics.113.150854>.
 - Kawano, M., and Nagata, S. (2018). Efferocytosis and autoimmune disease. *Int. Immunol.* 30, 551–558. <https://doi.org/10.1093/intimm/dxy055>.
 - Purice, M.D., Speese, S.D., and Logan, M.A. (2016). Delayed glial clearance of degenerating axons in aged *Drosophila* is due to reduced PI3K/Draper activity. *Nat. Commun.* 7, 12871. <https://doi.org/10.1038/ncomms12871>.
 - Spittau, B. (2017). Aging microglia-phenotypes, functions and implications for age-related neurodegenerative diseases. *Front. Aging Neurosci.* 9, 194. <https://doi.org/10.3389/fnagi.2017.00194>.
 - Cammarata-Mouchtouris, A., Acker, A., Goto, A., Chen, D., Matt, N., and Leclerc, V. (2022). Dynamic Regulation of NF- κ B Response in Innate Immunity: The Case of the IMD Pathway in *Drosophila*. *Biomedicines* 10, 2304. <https://doi.org/10.3390/biomedicines10092304>.
 - Melcarne, C., Lemaître, B., and Kurant, E. (2019). Phagocytosis in *Drosophila*: From molecules and cellular machinery to physiology. *Insect Biochem. Mol. Biol.* 109, 1–12. <https://doi.org/10.1016/j.ibmb.2019.04.002>.
 - Lukácsi, S., Farkas, Z., Saskó, É., Bajtay, Z., and Takács-Vellai, K. (2021). Conserved and distinct elements of phagocytosis in human and *C. elegans*. *Int. J. Mol. Sci.* 22, 8934. <https://doi.org/10.3390/ijms22168934>.
 - Hochreiter-Hufford, A., and Ravichandran, K.S. (2013). Clearing the dead: Apoptotic cell sensing, recognition, engulfment, and digestion. *Cold Spring Harbor Perspect. Biol.* 5, a008748. <https://doi.org/10.1101/cshperspect.a008748>.
 - Hilu-Dadia, R., and Kurant, E. (2020). Glial phagocytosis in developing and mature *Drosophila* CNS: tight regulation for a healthy brain. *Curr. Opin. Immunol.* 62, 62–68. <https://doi.org/10.1016/j.coi.2019.11.010>.
 - Hilu-Dadia, R., Hakim-Mishnaevski, K., Levy-Adam, F., and Kurant, E. (2018). Draper-mediated JNK signaling is required for glial phagocytosis of apoptotic neurons during *Drosophila* metamorphosis. *Glia* 66, 1520–1532. <https://doi.org/10.1002/glia.23322>.
 - Etchegaray, J.I., Elguero, E.J., Tran, J.A., Sinatra, V., Feany, M.B., and McCall, K. (2016). Defective phagocytic corpse processing results in neurodegeneration and can be rescued by TORC1 activation. *J. Neurosci.* 36, 3170–3183. <https://doi.org/10.1523/JNEUROSCI.1912-15.2016>.
 - Nakano, R., Iwamura, M., Obikawa, A., Togane, Y., Hara, Y., Fukuhara, T., Tomaru, M., Takano-Shimizu, T., and Tsujimura, H. (2019). Cortex glia clear dead young neurons via Drpr/dCed-6/Shark and Crk/Mbc/dCed-12 signaling pathways in the developing *Drosophila* optic lobe. *Dev. Biol.* 453, 68–85. <https://doi.org/10.1016/j.ydbio.2019.05.003>.
 - Draper, I., Mahoney, L.J., Mitsuhashi, S., Pacak, C.A., Salomon, R.N., and Kang, P.B. (2014). Silencing of DRPR leads to muscle and brain degeneration in adult *Drosophila*. *Am. J. Pathol.* 184, 2653–2661. <https://doi.org/10.1016/j.ajpath.2014.06.018>.
 - Tzou, P., Ohresser, S., Ferrandon, D., Capovilla, M., Reichhart, J.M., Lemaître, B., Hoffmann, J.A., and Immler, J.L. (2000). Tissue-specific inducible expression of antimicrobial peptide genes in *Drosophila* surface epithelia. *Immunity* 13, 737–748. [https://doi.org/10.1016/S1074-7613\(00\)00072-8](https://doi.org/10.1016/S1074-7613(00)00072-8).
 - Behnke, J.A., Ye, C., Setty, A., Moberg, K.H., and Zheng, J.Q. (2021). Repetitive mild head trauma induces activity mediated lifelong brain deficits in a novel *Drosophila* model. *Sci. Rep.* 11, 9738–9815. <https://doi.org/10.1038/s41598-021-89121-7>.
 - Sekiya, M., Wang, M., Fujisaki, N., Sakakibara, Y., Quan, X., Ehrlich, M.E., De Jager, P.L., Bennett, D.A., Schadt, E.E., Gandy, S., et al. (2018). Integrated biology approach reveals molecular and pathological interactions among Alzheimer's A β 42, Tau, TREM2, and TYROBP in *Drosophila* models. *Genome Med.* 10, 26. <https://doi.org/10.1186/s13073-018-0530-9>.
 - Coelho, D.S., Schwartz, S., Merino, M.M., Hauer, B., Topfel, B., Tietche, C., Rhiner, C., and Moreno, E. (2018). Culling Less Fit Neurons Protects against Amyloid-beta-Induced Brain Damage and Cognitive and Motor Decline. *Cell Rep.* 25, 3661–3673.e3. <https://doi.org/10.1016/j.celrep.2018.11.098>.
 - Wittmann, C.W., Wszolek, M.F., Shulman, J.M., Salvaterra, P.M., Lewis, J., Hutton, M., and Feany, M.B. (2001). Tauopathy in *Drosophila*: Neurodegeneration without neurofibrillary tangles. *Science* 293, 711–714. <https://doi.org/10.1126/science.1062382>.
 - Mosher, K.I., and Wyss-Coray, T. (2014). Microglial dysfunction in brain aging and Alzheimer's disease. *Biochem. Pharmacol.* 88, 594–604. <https://doi.org/10.1016/j.bcp.2014.01.008>.
 - Sierra, A., Abiega, O., Shahraz, A., and Neumann, H. (2013). Janus-faced microglia: Beneficial and detrimental consequences of microglial phagocytosis. *Front. Cell. Neurosci.* 7, 6–22. <https://doi.org/10.3389/fncel.2013.00006>.
 - Tremblay, M.E., and Sierra, A. (2014). Microglia in Health and Disease. <https://doi.org/10.1007/978-1-4939-1429-6>.
 - Cunningham, C., Campion, S., Lunnon, K., Murray, C.L., Woods, J.F.C., Deacon, R.M.J., Rawlins, J.N.P., and Perry, V.H. (2009). Systemic Inflammation Induces Acute Behavioral and Cognitive Changes and Accelerates Neurodegenerative Disease. *Biol. Psychiatr.* 65, 304–312. <https://doi.org/10.1016/j.biopsych.2008.07.024>.
 - Haruwaka, K., Ikegami, A., Tachibana, Y., Ohno, N., Konishi, H., Hashimoto, A., Matsumoto, M., Kato, D., Ono, R., Kiyama, H., et al. (2019). Dual microglia effects on blood brain barrier permeability induced by systemic inflammation. *Nat. Commun.* 10, 5816–5817. <https://doi.org/10.1038/s41467-019-13812-z>.
 - Michaud, M., Balardy, L., Moulis, G., Gaudin, C., Peyrot, C., Vellas, B., Cesari, M., and Nourhashemi, F. (2013). Proinflammatory cytokines, aging, and age-related diseases. *J. Am. Med. Dir. Assoc.* 14, 877–882. <https://doi.org/10.1016/j.jamda.2013.05.009>.
 - Perry, V.H. (2010). Contribution of systemic inflammation to chronic neurodegeneration. *Acta Neuropathol.* 120, 277–286. <https://doi.org/10.1007/s00401-010-0722-x>.
 - Barnes, D.E., and Yaffe, K. (2011). The projected effect of risk factor reduction on Alzheimer's disease prevalence. *Lancet Neurol.* 10, 819–828. [https://doi.org/10.1016/S1474-4422\(11\)70072-2](https://doi.org/10.1016/S1474-4422(11)70072-2).
 - Dumitrescu, A.L. (2016). Depression and inflammatory periodontal disease considerations-an interdisciplinary approach. *Front. Psychol.* 7, 347. <https://doi.org/10.3389/fpsyg.2016.00347>.
 - Cunningham, C. (2013). Microglia and neurodegeneration: The role of systemic inflammation. *Glia* 61, 71–90. <https://doi.org/10.1002/glia.22350>.
 - Lu, T.Y., MacDonald, J.M., Neukomm, L.J., Sheehan, A.E., Bradshaw, R., Logan, M.A., and Freeman, M.R. (2017). Axon degeneration induces glial responses through Draper-TRAF4-JNK signalling. *Nat. Commun.* 8, 14355–14359. <https://doi.org/10.1038/ncomms14355>.
 - Winkler, B., Funke, D., Benmimoun, B., Spéder, P., Rey, S., Logan, M.A., and Klämbt, C. (2021). Brain inflammation triggers

- macrophage invasion across the blood-brain barrier in *Drosophila* during pupal stages. *Sci. Adv.* 7, eabh0050. <https://doi.org/10.1126/sciadv.abh0050>.
43. Freeman, M.R., Delrow, J., Kim, J., Johnson, E., and Doe, C.Q. (2003). Unwrapping glial biology: Gcm target genes regulating glial development, diversification, and function. *Neuron* 38, 567–580. [https://doi.org/10.1016/S0896-6273\(03\)00289-7](https://doi.org/10.1016/S0896-6273(03)00289-7).
 44. Etchegaray, J.I., Timmons, A.K., Klein, A.P., Pritchett, T.L., Welch, E., Meehan, T.L., Li, C., and McCall, K. (2012). Draper acts through the JNK pathway to control synchronous engulfment of dying germline cells by follicular epithelial cells. *Development* 139, 4029–4039. <https://doi.org/10.1242/dev.082776>.
 45. MacDonald, J.M., Beach, M.G., Porpiglia, E., Sheehan, A.E., Watts, R.J., and Freeman, M.R. (2006). The *Drosophila* Cell Corpse Engulfment Receptor Draper Mediates Glial Clearance of Severed Axons. *Neuron* 50, 869–881. <https://doi.org/10.1016/j.neuron.2006.04.028>.
 46. Perkins, L.A., Holderbaum, L., Tao, R., Hu, Y., Sopko, R., McCall, K., Yang-Zhou, D., Flockhart, I., Binari, R., Shim, H.-S., et al. (2015). The transgenic RNAi project at Harvard Medical School: Resources and validation. *Genetics* 201, 843–852. <https://doi.org/10.1534/genetics.115.180208>.
 47. Zinke, I., Kirchner, C., Chao, L.C., Tetzlaff, M.T., and Pankratz, M.J. (1999). Suppression of food intake and growth by amino acids in *Drosophila*: The role of *pumpless*, a fat body expressed gene with homology to vertebrate glycine cleavage system. *Development* 126, 5275–5284. <https://doi.org/10.1242/dev.126.23.5275>.

STAR★METHODS

KEY RESOURCES TABLE

REAGENT or RESOURCE	SOURCE	IDENTIFIER
Antibodies		
Anti-GFP	Torrey Pines Biolabs	RRID:AB_10013661
Anti- Elav	Developmental Studies Hybridoma Bank	RRID:AB_528217
Anti-Repo	Developmental Studies Hybridoma Bank	RRID:AB_528448
Rabbit-Anti-Tyrosine Hydroxylase	Sigma-Aldrich	Cat# AB152; RRID:AB_390204
Chemicals, peptides, and recombinant proteins		
BODIPY	Invitrogen	Cat# D3922
Rhodamine Phalloidin	Invitrogen	Cat# R415
Vectashield with DAPI	Vector Laboratories	Cat# H1200
Critical commercial assays		
<i>In Situ</i> Cell Death Detection Kit, Fluorescein	Roche	Cat# 11684795910
Maxima First Strand cDNA Synthesis Kit for RT-qPCR	Thermo Scientific	Cat# K1671
Experimental models: Organisms/strains		
<i>Drosophila: drpr45</i>	Estee Kurant	
<i>Drosophila: UAS- Relish RNAi</i>	Vienna <i>Drosophila</i> Stock Center	Cat# 49414
<i>Drosophila: AttGFP</i>	Mitch Dushay	
<i>Drosophila: UAS-drpr RNAi</i>	Marc Freeman and Mary Logan	RRID:BDSC_67034
<i>Drosophila: UAS-LexA RNAi</i>	Bloomington <i>Drosophila</i> Stock Center	RRID:BDSC_67947
<i>Drosophila: repo-GAL4/TM3</i>	Bloomington <i>Drosophila</i> Stock Center	RRID:BDSC_7415
<i>Drosophila: elav-GAL4</i>	Bloomington <i>Drosophila</i> Stock Center	RRID:BDSC_458
<i>Drosophila: ppl-GAL4</i>	Michael O'Connor	RRID:BDSC_58768
<i>Drosophila: w[1118]</i>	Hermann Steller	RRID:BDSC_3605
Oligonucleotides		
RPL32 forward		ATGCTAAGCTGTCGCACAAATG
RPL32 reverse		GTTTCGATCCGTAACCGATGT
Attacin-A forward		CTCCTGCTGGAAAACATC
Attacin-A reverse		GCTCGTTTGGATCTGACC
Attacin-D forward		AGTGGGGGTCACTAGGGTTC
Attacin-D reverse		GTGGCGTTGAGGTTGAGATT
Diptericin forward		ACCGCAGTACCCACTCAATC
Diptericin reverse		GGTCCACACCTTCTGGTGAC
Software and algorithms		
FIJI/Image J		
Webknossos		
Neurodegeneration Vacuole Quantification	This study https://github.com/McCallLabBU/neurodegeneration_vacuole_quantification	
Prism	GraphPad	

RESOURCE AVAILABILITY

Lead contact

Further information and requests for reagents should be directed to and will be fulfilled by the lead contact, Kimberly McCall (kmccall@bu.edu).

Materials availability

This study did not generate new unique reagents.

Data and code availability

- All data in this paper can be requested by the lead contact.
- All original code has been deposited at the Github repository and is publicly available at https://github.com/McCallLabBU/neurodegeneration_vacuole_quantification.

EXPERIMENTAL MODEL AND SUBJECT DETAILS

Fly stocks and husbandry

The following fly strains were used: *drpr*⁴⁵ *FRT2A*,^{43,44} *UAS-Relish RNAi* (Vienna *Drosophila* Stock Center #49414), *AttGFP*²⁶ (provided by Dr. Mitch Dushay), *UAS-drpr RNAi*⁴⁵ (provided by Drs. Mary Logan and Marc Freeman), *UAS-LexA RNAi*⁴⁶ (Bloomington *Drosophila* Stock Center (BDSC) #67947), *repo-GAL4/TM3* (BDSC #7415), *elav-GAL4* (BDSC #458), *ppl-GAL4*⁴⁷ (provided by Dr. Michael O'Connor) and *w*¹¹¹⁸. All fly lines were raised at 25°C on standard cornmeal and molasses food. Aging flies were transferred to fresh food at least once per week.

METHOD DETAILS

Dissection and histology

Flies were anesthetized on CO₂ pads before dissection and equal numbers of male and female flies were dissected. Brains were dissected out of the cuticle in 4% paraformaldehyde (PFA) in phosphate-buffered saline with 0.1% Triton-X 100 (PBT) and transferred to 0.5 ml centrifuge tube with fresh dissection media. Whole heads were removed from bodies in fixation media (4% PFA in PBT). The proboscis was then removed, with care being taken not to damage the head. Heads were then placed in fresh fixation media and allowed to rot for 2-4 hours at room temperature. For whole body preparations, the wings, legs, and proboscis were removed and the abdomen was lightly punctured in fixation media (4% PFA in PBT). Flies were then placed in fresh fixation media and incubated at room temperature with rotation for 4 hours.

For cryosectioning after dissection, PFA was removed and replaced with PBT for up to an hour. PBT was then removed and replaced with 15% sucrose in PBT. Heads or bodies were incubated for 48 hours in sucrose at 4°C with rotation. 15% sucrose was then replaced with 30% sucrose in PBT, and tissues were incubated for a further 48 hours at 4°C with rotation. Tissues were then embedded in optimal cutting temperature (OCT) media (Fisher #23-730-571) in aluminum foil molds and frozen on powdered dry ice, before being stored at -80°C until sectioning. Tissues were sectioned at -19 to -21°C, with heads at a thickness of 18 μm and whole bodies at 25 μm unless noted otherwise.

Staining procedures

For whole mount staining, dissected brains were incubated for 50 minutes in fresh fixation media at room temperature. Samples were then permeabilized in three washes for a total of up to one hour in 1X PBT at room temperature. Samples for antibody staining were incubated in PBANG (PBT, bovine serum albumin (BSA), and normal goat serum (NGS)) for one hour at room temperature or overnight at 4°C. Samples were then incubated with primary antibody diluted in PBANG for 4-5 days at 4°C with rotation. Samples were then washed in PBT for a total of one hour, before being incubated in secondary antibody diluted in PBANG for 4 hours at room temperature or two days at 4°C in the dark with rotation. Samples were then transferred to Vectashield with DAPI (Vector Laboratories) and stored in the dark at 4°C until mounting on slides.

Sections on slides were washed in coplin staining jars in PBS before being incubated for two hours in primary antibody diluted in PBS. Slides were then washed twice in PBS for up to one hour before being incubated for 45 minutes in secondary antibody diluted in PBS. Slides were then again washed at least three times in PBS for a total of one hour. Coverslips were then mounted with two drops of Vectashield with DAPI (Vector Laboratories), then sealed with nail polish.

The following primary antibodies were used: Anti-GFP (Torrey Pines Biolabs Cat# TP401 071519, RRID:AB_10013661, 1:100), Anti-Elav (DSHB Cat# Elav-9F8A9, RRID:AB_528217, 1:100) and Anti-Repo (DSHB Cat# 8D12 anti-Repo, RRID:AB_528448, 1:100), Anti-Tyrosine Hydroxylase (Sigma-Aldrich Cat# AB152, RRID:AB_390204, 1:200). Secondary antibodies were obtained from Jackson Laboratories and were used at 1:200 or 1:400.

For BODIPY (lipid) staining, whole tissues were dissected, fixed, and permeabilized as described above, and were incubated at room temperature in the dark in a solution of 1:1000 of 1mg/ml BODIPY (Invitrogen, D3922) diluted in DMSO:1X PBS for 2 hours. Samples were then washed three times in PBS and stored in Vectashield with DAPI until coverslipping. After sectioning and washing in PBS as described above, sections on slides were incubated in a solution of 1:1000 of 1mg/ml BODIPY diluted in DMSO:1X PBS for 45 minutes at room temperature or overnight at 4°C, protected from light. Slides were then washed three times with 1X PBS, then a coverslip was added as described above.

For whole-mount phalloidin staining, whole brains were dissected, fixed, and permeabilized as described above, and were incubated at 4°C in the dark in a solution of 1:100 of rhodamine phalloidin (Invitrogen, R415) diluted in PBT overnight. Samples were washed three times briefly in PBS and mounted as described above.

TUNEL staining

The *In Situ* Cell Death Detection Kit, Fluorescein (Roche, Cat# 11684795910) was used. Briefly, after fixing and washing as for antibody staining, tissue was permeabilized in PBT at 4°C overnight while rotating. Tissue was further permeabilized in freshly made 0.1% sodium citrate in PBT for 30 min at 65°C. Samples were then incubated in 30 μ l TUNEL reaction mixture (27 μ l label solution and 3 μ l enzyme solution) for 3 hours at 37°C. Samples were washed three times in PBS while rotating for a total of 30 min. Samples were then placed in VectaShield with DAPI overnight and mounted on slides. To quantify the number of TUNEL-positive cells, we used the cell counter plugin in Fiji. One-way ANOVA with Dunnett's test was used for statistical analysis.

Microscopy

Samples were visualized by either fluorescence and light microscopy (Olympus BX-60) or confocal microscopy (Olympus FluoView FV10i, or Nikon C2Si). Image analysis was performed using ImageJ/FIJI and image processing for figure production was performed using Adobe Photoshop or Adobe Illustrator.

To visualize neurodegenerative holes in a whole-mount brain, a 2-photon microscope (Prairie Technologies Ultima) was used. The laser used was a Spectra Physics Mai Tai (80MHz pulse rate) and was operated at 815 nm wavelength. The objective was a 20X Olympus lens with a numerical aperture of 1.00 and a working distance of 2 mm. Z-stacks were acquired at 1 μ m using the Prairie acquisition software with the resolution of 1024 x 1024 pixels. Images were processed through Fiji and Webknossos.

RT-PCR

Flies were aged in groups of 15 males and 15 females until the appropriate age was reached. Flies were then placed in cryovials and snap-frozen in liquid nitrogen in groups of ~30. Flies were stored at -80°C until ready for use, or processed immediately. Frozen flies were decapitated by vortexing for 10 seconds, placing back in liquid nitrogen, and then repeating the process one more time. Heads were separated from bodies rapidly using a paintbrush, over liquid nitrogen. Heads were then homogenized in QIAlysis solution. RNA was then extracted using the Qiagen RNeasy kit. The final concentration of RNA from this process was about 80 ng/ μ l for 30 heads. RNA was stored at -80°C until cDNA synthesis.

The Maxima First Strand cDNA Synthesis Kit for RT-qPCR (Thermo Scientific, K1671) was used to produce cDNA. Kit components and samples were thawed on ice, and RNA concentration was determined using a NanoDrop. Sterile, RNase-free tubes on ice were used for reactions. To each tube, the following were added: 1 μ l of 10X dsDNase buffer, 1 μ l of dsDNase, 0.1 μ g of total RNA, and nuclease-free water to reach 10 μ l. Reactions were gently mixed and briefly centrifuged on a table-top centrifuge. Reactions were then incubated at 37°C for 2 minutes, then chilled on ice. The following components were then added to each tube: 4 μ l of 5X Reaction Mix, 2 μ l of Maxima Enzyme Mix, and 4 μ l of nuclease-free water. Reactions were gently mixed and briefly centrifuged on a table-top centrifuge. Reactions were then incubated for 10 minutes at 25°C, followed by 15 minutes at 50°C, then 5 minutes at 85°C. The reaction products were then immediately used for RT-qPCR.

The GoTaq qPCR Master Mix (Promega, A6001) was used to perform RT-qPCR. cDNA was diluted to 5 ng/ μ l, and primers diluted to 10 mM. Kit components were thawed on ice. In nuclease-free tubes on ice, master mixes were prepared for each primer. In a 384-well plate, 2 μ l of cDNA was loaded into each well (except NTC, in which water was added instead). 8 μ l of Master Mix for the appropriate primer set was then added to each well. The plate was sealed with a clear plate cover, then briefly centrifuged. Samples were then analyzed in an ABI 7900ht real time PCR machine.

QUANTIFICATION AND STATISTICAL ANALYSIS

To measure Attacin-GFP expression in the fat body, the fat body area was first defined using cell morphology, anatomy, and DAPI. The region of interest was outlined in FIJI. A minimum threshold was determined using the center areas of the brain as a measure for background. The % of the fat body area which was above the threshold was then measured and recorded. Sections which were folded, improperly stained, or overly damaged were discarded.

To measure neurodegeneration, cryosection and whole-mount brain imaging²⁷ were used. Heads were cryosectioned and stained with BODIPY as described above. Sections were imaged by confocal microscopy as outlined above. Images were converted to PNG files in FIJI, then opened in Adobe Photoshop for vacuole counting. Vacuoles larger than four microns in diameter were counted, using the brush tool as a size guide. At least two sections per brain were analyzed. Sections with most of the central brain and optic lobe were selected for counting, and sequential sections were not used, to avoid counting the same vacuoles twice. Researchers were blinded to genotype. Vacuoles located in the retina were not counted. Any cracks in the tissue were not counted, as these result from processing.

For whole-mount brain analysis done with 2-photon microscopy, images were converted to RGB Z-stacks in FIJI, then imported to Webknossos for vacuole segmentation and three-dimensional geometric analysis. Areas devoid of staining were identified as vacuoles using the "quick select" automatic segmentation tool. Segmentation was performed for selected layers of the Z-stack and volume interpolation was performed to annotate the vacuole regions within the segmentation layers. 3D meshes were computed for volume interpolated vacuoles in Webknossos and exported as .stl files for downstream analysis. Vacuoles in both the central brain and optic lobes were included in the analysis for all samples. Total number of vacuoles per sample and the percentage of whole brain volume occupied by vacuoles were determined using the numpy-stl python package. Scipy python package was used to perform one-sided independent samples t-test. Jupyter

notebook used for measuring and visualizing 3D mesh volumes, and performing the statistical analysis are available on the Github repository https://github.com/McCallLabBU/neurodegeneration_vacuole_quantification.

All statistical analyses were performed using Prism software. For RT-qPCR in Figure 1, unpaired t-tests with Welch correction were performed on log-transformed delta-delta-CT values and samples were normalized with Rpl32. For RT-qPCR in Figure S1, two-way ANOVA with Tukey test were performed on delta-delta-CT values and samples were normalized with Rpl32. For determining the % of fat body positive for GFP, unpaired t-tests were performed. For measuring neurodegeneration using cryosectioning, Brown-Forsythe and Welch ANOVA and unpaired t tests with Welch correction were performed. For measuring dopaminergic neurons and TUNEL-positive cells, one-way ANOVA with Dunnett's posttest were performed. P-values are indicated by asterisks in figures as follows: * $p < 0.05$, ** $p < 0.01$, *** $p < 0.001$, **** $p < 0.0001$.